1521-0111/100/1/73–82$35.00
MOLECULAR PHARMACOLOGY

https://doi.org/10.1124/molpharm.120.000195
100:73–82, July 2021

Automated Intracellular Pharmacological Electrophysiology for Ligand-Gated Ionotropic Receptor and Pharmacology Screening[S]

Riley E. Perszyk, Mighten C. Yip, Ona L. McConnell, Eric T. Wang, Andrew Jenkins, Stephen F. Traynelis, and Craig R. Forest

George W Woodruff School of Mechanical Engineering, Georgia Institute of Technology, Atlanta, Georgia (R.E.P., M.C.Y., C.R.F.); Department of Pharmacology and Chemical Biology, Emory University School of Medicine, Atlanta, Georgia (R.E.P., A.J., S.F.T.); Department of Molecular Genetics & Microbiology, Center for Neurogenetics, Genetics Institute, University of Florida, Gainesville, Florida (O.L.M., E.T.W.); and Department of Anesthesiology, Emory University, Atlanta, Georgia (A.J.)

Received October 28, 2020; accepted April 8, 2021

ABSTRACT

Communication between neuronal cells, which is central to brain function, is performed by several classes of ligand-gated ionotropic receptors. The gold-standard technique for measuring rapid receptor response to agonist is manual patch-clamp electrophysiology, capable of the highest temporal resolution of any current electrophysiology technique. We report an automated high-precision patch-clamp system that substantially improves the throughput of these time-consuming pharmacological experiments. The patcherBot$_{Pharma}$ enables recording from cells expressing receptors of interest and manipulation of them to enable millisecond solution exchange to activate ligand-gated ionotropic receptors. The solution-handling control allows for autonomous pharmacological concentration-response experimentation on adherent cells, lifted cells, or excised outside-out patches. The system can perform typical ligand-gated ionotropic receptor experimentation protocols autonomously, possessing a high success rate in completing experiments and up to a 10-fold reduction in research effort over the duration of the experiment. Using it, we could rapidly replicate previous data sets, reducing the time it took to produce an eight-point concentration-response curve of the effect of propofol on GABA type A receptor deactivation from likely weeks of recording to ~13 hours of recording. On average, the rate of data collection of the patcher Bot$_{Pharma}$ was a data point every 2.1 minutes that the operator spent interacting with the patcherBot$_{Pharma}$. The patcherBot$_{Pharma}$ provides the ability to conduct complex and comprehensive experimentation that yields data sets not normally within reach of conventional systems that rely on constant human control. This technical advance can contribute to accelerating the examination of the complex function of ion channels and the pharmacological agents that act on them.

SIGNIFICANCE STATEMENT

This work presents an automated intracellular pharmacological electrophysiology robot, patcherBot$_{Pharma}$, that substantially improves throughput and reduces human time requirement in pharmacological patch-clamp experiments. The robotic system includes millisecond fluid exchange handling and can perform highly efficient ligand-gated ionotropic receptor experiments. The patcherBot$_{Pharma}$ is built using a conventional patch-clamp rig, and the technical advances shown in this work greatly accelerate the ability to conduct high-fidelity pharmacological electrophysiology.

Introduction

Patch-clamp electrophysiology is an incredibly important technique that has enabled many discoveries in pharmacology, physiology, and neuroscience (Neher and Sakmann 1976; Suk et al., 2019). Patch-clamp recording has the ability to accurately measure the time course of postsynaptic or postjunctional currents and can fully resolve ion flux and the rapid transitions of individual ionotropic receptors (Neher and Sakmann, 1976; Colquhoun and Sigworth, 1995; Auerbach and Zhou, 2005; Chakrapani et al., 2011). However, extensive effort and time are required to perform this high-resolution technique. Many alternative methods and machines have been developed that attempt to accelerate the collection of data that approximate

C.R.F. was supported by National Institutes of Health National Institute of Mental Health [Grant U01-MH106027], National Institute of Neurological Disorders and Stroke [Grant R01-NS102727], National Eye Institute [Grant R01-EY023173], and National Institute on Drug Abuse [Grant T90-DA032466]. S.F.T. was supported by National Institutes of Health National Institute of Neurological Disorders and Stroke [Grant R35-NS111619]. A.J. was supported by National Institutes of Health National Institute of Neurological Disorders and Stroke [Grant R01-NS089719 and R01-NS111280], National Institute of Mental Health [Grant R01-MH117315] and the Marigold Foundation.

[S] This article has supplemental material available at molpharm.aspetjournals.org.
https://doi.org/10.1124/molpharm.120.000195.

ABBREVIATIONS: GABA, Y-aminobutyric acid; GABA$_A$R, GABA type A receptor; GFP, green fluorescent protein; GluN, NMDAR subunits; HEK, human embryonic kidney; MEM, minimum essential media; NMDA, N-methyl-D-aspartate; NMDAR, *N*-methyl-D-aspartate receptor; PRO, propofol.

what patch-clamp electrophysiology can achieve, such as activity-sensitive fluorometric probes and high-throughput machines that patch dissociated cells on planar patch-clamp "chips" (Ai, 2015; Yu et al., 2016; Deo and Lavis, 2018; Obergrussberger et al., 2018; Liu et al., 2019; Mollinedo-Gajate et al., 2019). However, these methods sacrifice the high precision of patch-clamp electrophysiology to achieve higher throughput. For instance, fluorometric probes must be tuned to a specific application, and fully resolving the kinetics or full activity of ionotropic receptors is typically not possible. Imaging experiments also cannot control for confounding voltage fluctuation associated with the measured response. Additionally, for high-throughput patch-clamp systems, performance is limited by their solution-handling capabilities, and cost of both equipment and supplies is prohibitive for many studies. Most of these methods are also incapable of measuring cells that are adherent or embedded in tissue (Suter et al., 2010; Campagnola et al., 2014; Annecchino et al., 2017; Wu and Chubykin, 2017; Obergrussberger et al., 2018).

Recently, our group has worked on equipping a traditional intracellular electrophysiology rig with the capability to operate autonomously (Kolb et al., 2016, 2019). Robotic vision, pipette pressure control, and electrode cleaning enable the resulting patcherBot to execute the basic steps required to perform patch-clamp electrophysiology without human intervention. Utilizing these automated methods allows for the acceleration of electrophysiology experimentation by reducing the process times of many steps as well as drastically decreasing the amount of required operator-rig interfacing time. The patcherBot is capable of patching over 30 cells sequentially, can run unattended for over 4 hours, and operates at about a 70% success rate (reaching the whole-cell patch-clamp configuration per patching attempt) (Kolb et al., 2019). These advances enable the patcherBot to record spontaneous activity or voltage-dependent biologic phenomena, and they can be multiplexed within a single preparation to record from multiple cells simultaneously. Thus, the patcherBot is highly proficient at addressing questions such as connectomics or intrinsic properties of neurons. Despite its many capabilities, this technology cannot perform many assays on ligand-gated ionotropic receptors or pharmacological studies.

Here, we present an implementation of the patcherBot that enables automated intracellular pharmacological electrophysiology (Fig. 1). The patcherBot$_{Pharma}$ can perform pharmacological concentration-response experiments and can record ligand-gated ionotropic receptor response to fast agonist exposure (millisecond exchange time) with automated control of the microscope, bath solution, a solution manifold, and a piezoelectric translator. We observe a high-throughput rate of the patcherBot$_{Pharma}$ unattended, with further improvement using minimal operator assistance. We show the capabilities of the patcherBot$_{Pharma}$ by replicating a conventional data set substantially faster—with considerably less human effort—than we had done previously. The increased efficiency enabled by

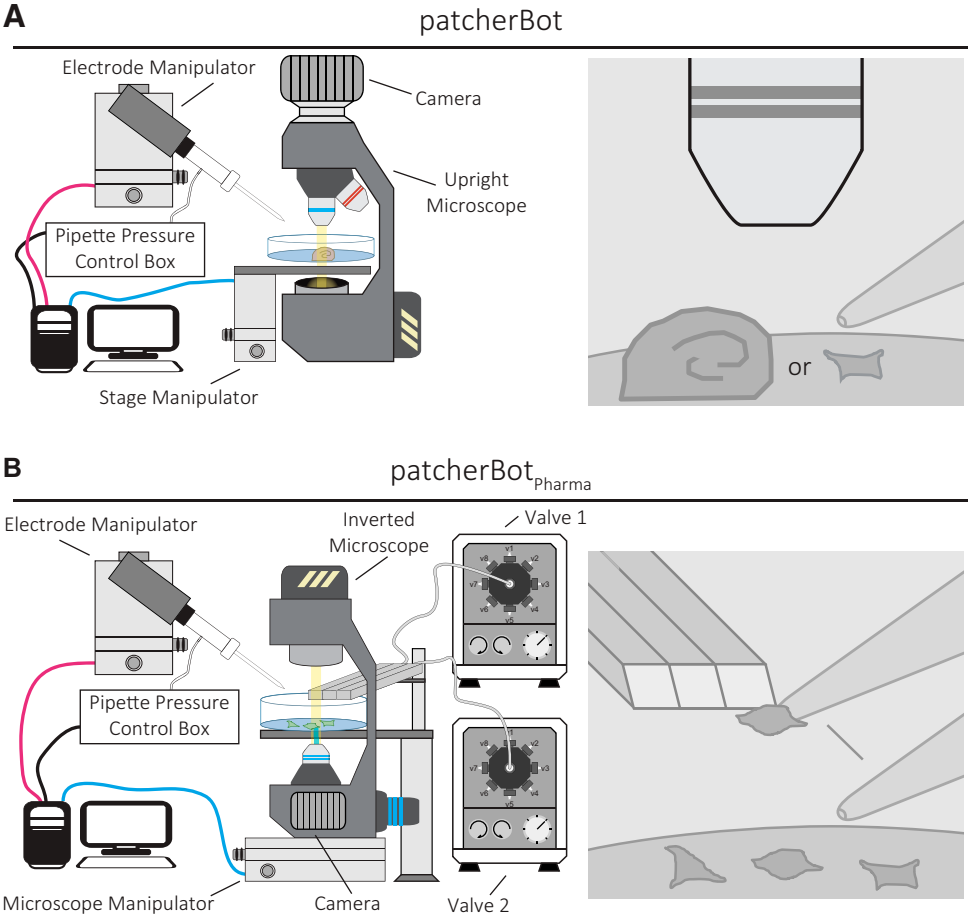

Fig. 1. Comparison of patcherBot vs. patcherBot$_{Pharma}$. (A) Cartoon of the previously published patcherBot (Kolb et al., 2019), assembled from an upright microscope, high sensitivity camera, custom pressure control box, quasi-four-axis electrode manipulator, and a motorized stage. (B) Cartoon of the patcherBot$_{Pharma}$, assembled from an inverted microscope, high sensitivity camera, custom pressure control box, quasi-four-axis electrode manipulator, a motorized microscope manipulator, two solution valves, and a solution exchange manifold. A manual detailing the components and the operation of the patcherBot$_{Pharma}$ is provided on GitHub (https://github.com/riley-perszyk/patcherBot_pharma).

this patch-clamp electrophysiology system creates the potential to address scientific questions that were previously considered impractical because of large, time-consuming requirements needed to complete data acquisition using conventional approaches.

Materials and Methods

patcherBot$_{Pharma}$ Hardware and Software. The patcher Bot$_{Pharma}$ is built on a standard inverted microscope (Axiovert 200; Zeiss) to allow for clearance of the recording electrode and solution-handling manifolds. Standard, three-axis micromanipulators were used to translate the recording electrode (PatchStar; Scientifica) and the microscope [Motorized XY Stage (Universal Motorised Stage) with Z-focus module; Scientifica]. A high-sensitivity camera (Retiga Electro; QImaging) is used for computer vision. Electrode pressure was controlled using a custom control box that regulates house-air line to deliver −700 to +1000 mbar using an inline venturi tube (SMC Pneumatics), solenoid valve (Parker Hannifin), and a digital air regulator (ProportionAir) controlled by an Arduino Uno for rapid pressure switching (Kodandaramaiah et al., 2012; Kolb et al., 2016, 2019). A three-barreled, square cross-section solution manifold (3SG700-5; Warner Instruments) attached to a piezoelectric translator (Burleigh Instruments) was used for cell perfusion, similar to many that have been previously published (Glasgow and Johnson, 2014; MacLean, 2016). Barrels of the solution manifold were connected to eight-valve solution changers (Hamilton Modular Valve Positioner). Custom LabVIEW code (National Instruments) integrating manipulators (electrode and microscope), camera view of the microscope stage, pressure control box, piezoelectric translator, and solution valves was implemented to control the rig and enable automated experimentation (Fig. 1A). Communication between the computer and the amplifier, piezoelectric translator, and solution changers was achieved using a data acquisition device (DAQ, BNC-2110; National Instruments) with several analog and digital interfaces. The patcherBot$_{Pharma}$ LabVIEW code can be found on GitHub (https://github.com/riley-perszyk/patcherBot_pharma), along with a manual detailing the components and the operation of the system.

Transiently Expressing Human Embryonic Kidney Cells. HEK-293 cells (CRL 1573; American Type Culture Collection; hereafter HEK cells) and a stable GABA$_A$R-expressing cell line were cultured in Dulbecco's modified Eagle's medium (10566016; ThermoFisher Scientific) supplemented with 10% FBS, 10 U/ml penicillin, and 10 μg/ml streptomycin and maintained at 5% CO_2 in a 37°C incubator. For use on the electrophysiology rig, heterologous cells were plated on poly(D-lysine)–coated glass coverslips (0.1–0.5 mg/ml; Warner Instruments). Recombinant NMDARs were transiently expressed from cDNA encoding rat GluN 1-1a (hereafter GluN1, U08261) and GluN2A (D13211). Calcium phosphate was used to transfect HEK cells in a 24-well plate with 500 ng of DNA at a ratio of 1:1:5 (GluN1:GluN2A:GFP). At 4 hours after transfection, NMDAR antagonists DL-2amino-5-phosphonovalerate (200 μM, DL-APV) and 7-chlorokynurenic acid (200 μM) were added to the culture medium to decrease the cytotoxic effect of NMDAR expression.

Stably Expressing HEK Cells. cDNAs for mouse *Gabra1*, *Gabrb2*, and the long form of *Gabrg2* were subcloned into the pAC156 plasmid, a generous gift from Albert Cheng. The cDNAs were driven by an EF1α promoter. A PGK promoter-driven puromycin resistance cassette was also present in pAC156; both cassettes were flanked by piggybac transposon arms. All three plasmids were cotransfected with the mPB piggybac transposase into HEK 293 cells, selected by puromycin, and sorted into single cells. Clones were assayed for Gabra1, Gabrb2, and Gabrg2 expression by immunofluorescence, and one clone was expanded for further study and use in this manuscript. Trypsin was used to dissociate the cells and plated on the same coverslips, as mentioned above, 24–72 hours before experimentation [shorter time and less poly(D-lysine) for lifted cell and the inverse for excised patches].

Primary Neuronal Culture. Primary cortical neurons were cultured from rat embryos (embryonic day 17.5), of either sex, as previously described (Perszyk et al., 2020). Briefly, cortices were dissected from the embryos and trypsinized (0.25%, 37°C). After rinsing cortical particles with warm Hanks' balanced salt solution (containing 10 mM HEPES, 2 rinsed), the particles were homogenized in minimum essential media (MEM; Cellgro) containing 10% FBS (MEM/FBS). Cells were plated on coverslips coated with 0.5–1 mg/ml poly(L-lysine) in MEM/FBS. At 2 hours after plating, media were removed and replaced with glia-conditioned Neurobasal medium (Life Technologies; incubated on secondary mouse glia for 24 hours) with 1× Glutamax (Life Technologies) and 1× B-27 (Life Technologies). Neurons were cultured at 5% CO_2 and 37°C, and every 3 to 4 days, a 50% media replacement was performed. Neurons were used at 14–21 days *in vitro*. These procedures were approved by the Emory University Institutional Animal Care and Use Committee, and they were performed in accordance with state and federal Animal Welfare Acts and the policies of the Public Health Service.

Whole-Cell Voltage-Clamp Recordings. Whole-cell voltage-clamp recordings were performed with thin-walled borosilicate glass electrodes (3–6 MΩ, TW150F-4; World Precision Instruments) filled with solution containing (in mM) 110 Cs-gluconate, 30 CsCl, 5 HEPES, 4 NaCl, 0.5 $CaCl_2$, 2 $MgCl_2$, 5 1,2-bis(*o*-aminophenoxy)ethane-*N*,*N*,*N*′,*N*′-tetraacetic acid, 2 NaATP, and 0.3 NaGTP (pH 7.35). The extracellular recording solution contained (in mM) 150 NaCl, 10 HEPES, 3 KCl, 0.5 $CaCl_2$, 1 $MgCl_2$, and 0.01 EDTA (pH 7.4). Whole-cell recordings from primary cortical neurons (examples of alternative experiment paradigms are shown in the Supplemental Figure 2) were obtained utilizing an internal solution [containing (in mM) 115 K-gluconate, 20 KCl, 10 HEPES, 2 Mg_2ATP, 0.3 NaGTP, and10 Na_2-phosphocreatine (pH 7.35)] and external solution stated above but with 1 mM $CaCl_2$. The electrode cleaning solution (2% Tergazyme in water) was made fresh daily. Cleaned electrodes were washed in appropriate internal solution. All solutions were filtered (0.45 μm or 0.22 μm). Responses were recorded using a Multiclamp 700B (Molecular Devices), filtered at 10 kHz (−3 dB), and digitized at 20 kHz.

Analysis and Statistics. Whole-cell rapid solution exchange experiments were analyzed using custom algorithms (Matlab; Mathworks). The desensitization and deactivation time courses were fitted by exponential functions based on receptor type. For NMDAR desensitization and GABA$_A$R deactivation, they were fit by one exponential function,

$$I = A * e^{\frac{-time}{\tau}} + C,$$

where I was the current response, A was the amplitude of the response, *time* is the duration after the peak response or removal of agonist, τ is the time constant, and C is an offset constant. NMDAR deactivation and GABA$_A$R desensitization were fit with a dual exponential function:

$$I = A_f * e^{\frac{-time}{\tau_f}} + A_s * e^{\frac{-time}{\tau_s}} + C.$$

The two exponentials are designated as fast (A_f, τ_f) and slow (A_s, τ_s). For dual exponential fits, a weighed tau (τ_w) was calculated:

$$\tau_w = \frac{A_f * \tau_f + A_s * \tau_s}{A_f + A_s}.$$

The Fisher's exact test, two tailed, was used where noted. Means ± S.E.M. are used unless otherwise noted.

Results

For efficient traditional pharmacological experimentation, one must ensure the viability of the available cell pool during sequential experimentation. Especially for ligand-gated ionotropic receptors, this is achieved by lifting cells or pulling patches from the coverslip and performing solution application far from the cells remaining on the coverslip (Fig. 2B). This procedure can be more straightforward than translating the manifold to the cell locations. We first set out to ensure that this could be done reproducibly by the robotic system, since achieving accurate placement of all components is essential for efficient data collection with minimal operator effort. We first verified that the patcherBot$_{Pharma}$ could traverse the recording electrode distances on the millimeter scale while ensuring micrometer-scale precision at the interface of a multibarrel flow pipe, given that piezoelectric translators typically have a maximum range of 100–300 μm. This is especially important since in one complete cycle of the patcherBot$_{Pharma}$ operation (patching, experiment manipulation, and electrode cleaning) the electrode will translate roughly 150 mm.

The patcherBot$_{Pharma}$ needs to achieve this high level of accuracy and precision at the solution manifold without necessitating manual, time-intensive error correction. Typically, the placement of the electrode at the solution interface is established visually at a predesignated location (beginning of the recording session), and then test pulses are conducted to ensure proper placement, taking at least 30 seconds for a highly skilled operator. To test the ability to return to the critical location, we translated the electrode through the various positions required to patch sequentially (4×). After each cycle, the solution exchange around an open-tip electrode was measured by triggering a piezoelectric translation of the solution manifold (exchanging extracellular buffer and a partial salt solution containing 50% extracellular buffer and 50% H_20). We found that the electrode could be repeatably positioned while retaining the fast solution exchange time and without placement errors that can lead to recording artifacts (i.e., straying into the adjacent lane before the jump; Fig. 2C).

Lifting cells in the whole-cell configuration and pulling outside-out patches are two of the most common methods of

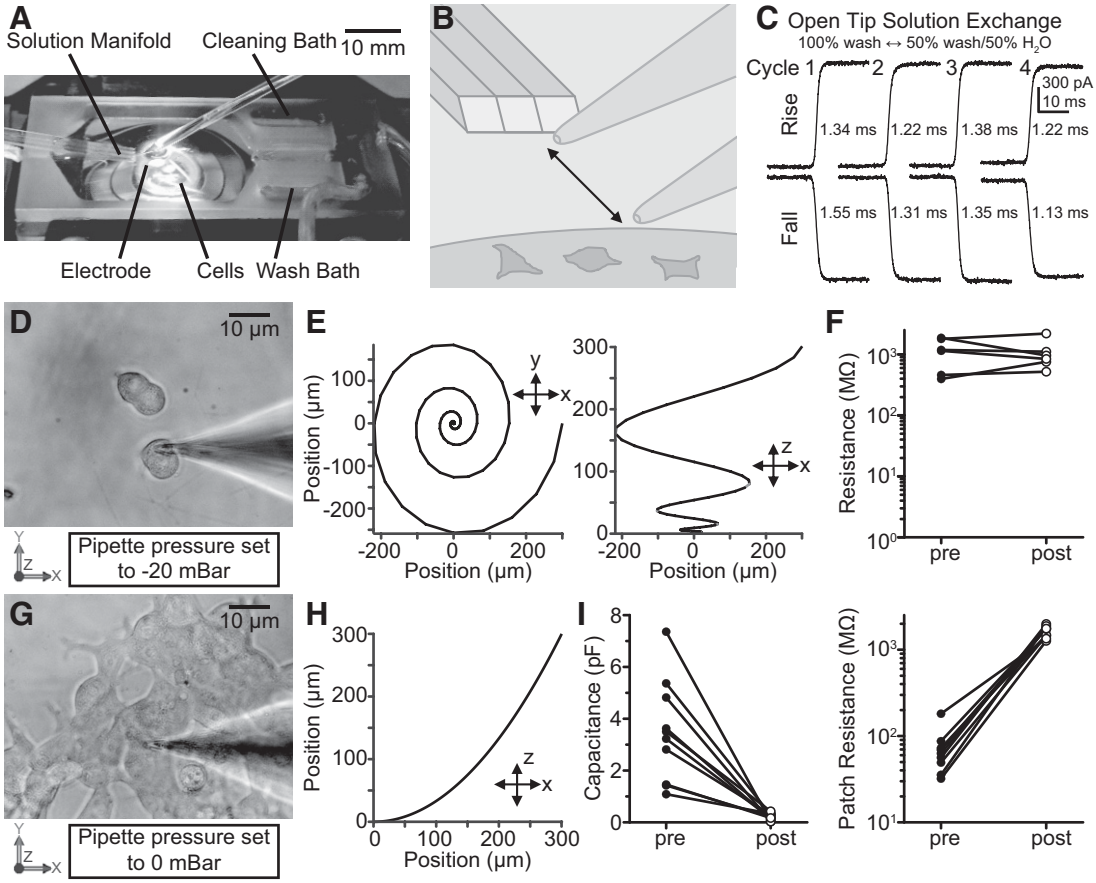

Fig. 2. Repeatability of the physical manipulations required for fast solution exchange electrophysiological experiments. (A) Image of the recording chamber. (B) Cartoon illustrating the large distances (e.g., X-Y mm scale) the electrode must translate during experimentation. (C) Open-tip solution exchange times, using piezoelectric translator, across many repeated experimental cycles (cell locations, solution manifold interface, cleaning/wash bath). (D–F) Cell lifting procedure. (D) Image of an isolated cell in the whole-cell conformation before lifting (isolated cells are more reliably lifted than those with cellular processes to adjacent cells). (E) Spiral path (100 discrete segments) employed to lift isolated cells. (F) Resulting resistance plot showing a high-resistance seal is robustly maintained during the lifting process. (G–I) Patch-pulling procedure. (G) Image of a cell in the whole-cell conformation before pulling an outside-out patch. (H) Arc path (100 discrete segments) employed to pull outside-out patches. (I) Resulting capacitance and resistance plots showing successful high-resistance, low-capacitance outside-out patches. We speculate the low resistance prior to pulling the outside-out patches is due to electrical connections due to gap-junctions between multiple cultured cells in physical contact with one another.

studying ligand-gated ionotropic receptors using rapid solution exchange manifolds. For lifting cells in the whole-cell conformation, we implemented a segmented (100 step) spiral translation method while applying a light suction on the pipette (−40 mbar; Fig. 2, D and E). In applying this method, we were able to reliably lift cells while retaining the high-resistance seal that was obtained while breaking through (Fig. 2F). For pulling outside-out patches, we implemented a segmented (100 step) arc translation method while the pipette was at atmospheric pressure (Fig. 2, G and H). In applying this method, we were able to repeatedly pull outside-out patches, achieving the characteristic low capacitance and high resistance of this patch-clamp conformation (Fig. 2I).

With these new functionalities, this system proved capable of performing rapid solution exchange experiments as well as executing precise solution application. To demonstrate these capabilities, we recorded from two synaptic ligand-gated ionotropic receptors, $GABA_AR$ and NMDARs, using the $patcherBot_{Pharma}$ (Fig. 3; Table 1). As expected, the $patcherBot_{Pharma}$ was capable of recording NMDAR responses from transiently transfected HEK cells that were lifted off the bottom as well as from outside-out patches excised from HEK cells (Fig. 3A). Additionally, the $patcherBot_{Pharma}$ was capable of recording $GABA_AR$ responses from stably expressing cells, including both long agonist applications as well as brief agonist applications (5 milliseconds; Fig. 3B). In addition to this experimental protocol, the $patcherBot_{Pharma}$ is programmed to conduct many other commonly used solution exchange protocols (Supplemental Fig. 1) as well as voltage-clamp and current-clamp protocols. These can be employed to measure neuronal activity or study specific voltage-gated channels expressed in heterologous cells. The $patcherBot_{Pharma}$ can implement these experimental protocols on adherent cells, lifted cells, or patches pulled from cells, paired with solution control to measure channel responses in different conditions (Supplemental Fig. 2).

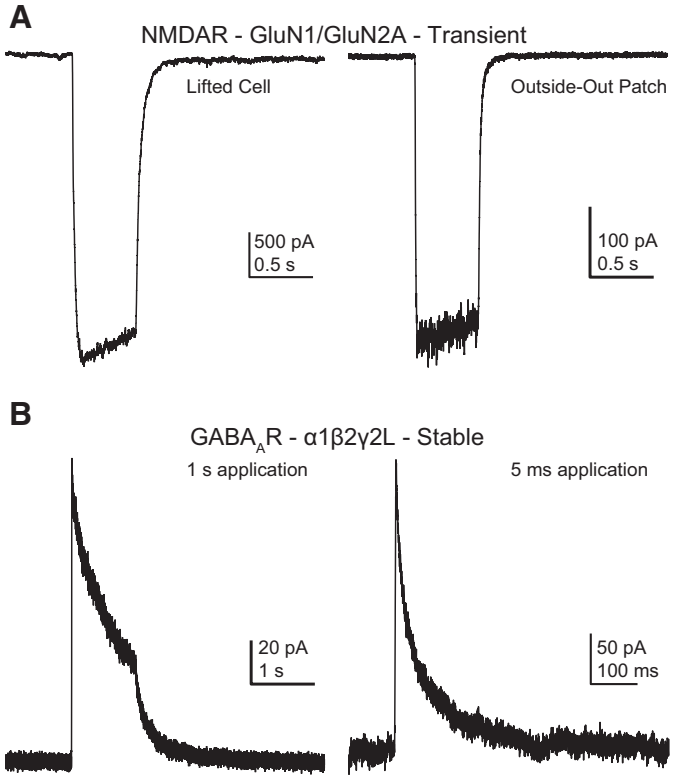

Fig. 3. Exemplary fast solution exchange electrophysiological experimental results. (A) NMDAR responses from transiently transfected HEK cells stimulated by 100 μM glutamate and 30 μM glycine. Recordings are from a lifted whole cell (left) and an outside-out patch using a 4-MΩ electrode (right) at −60 mV in 0 mM Mg^{2+}. (B) $GABA_AR$ responses from stably transfected HEK cells ($\alpha1\beta2\gamma2L$) stimulated by 1 mM GABA. Recordings are from a lifted whole cell (left, 1-second application) and an outside-out patch (right, 5-millisecond application).

We subsequently performed a series of pharmacology experiments on $GABA_AR$ and NMDARs in which we recorded rapid agonist application to excised outside-out patches to assess $patcherBot_{Pharma}$ performance on the minimum processes required in an experiment (Supplemental Table 1). Assessment of the overall performance of the $patcherBot_{Pharma}$ for both glutamate and GABA receptors revealed that a giga-ohm resistance patch (gigaseal patch) was obtained 81.2% of the time (108 of 133 attempts). After a gigaseal was achieved, successful break-in occurred 96.3% of the time to establish the whole-cell conformation (104 of 108 gigaseals). After whole-cell configuration stabilization, the success rate of excising an outside-out patch was 76.0% (79 of 104 whole-cell conformations). The successful completion of an experiment based on every outside-out patch pulled was 74.7% (59 of 79 outside-out patches). Subsequent failure to complete an experiment after obtaining an outside-out patch was due to either the lack of detectable receptor response upon agonist application or patch integrity breakdown after initiating the experimental recordings. Taken together, the overall success of the $patcherBot_{Pharma}$ was 44.4% (59 of 133 attempts). In examining the nature of failed experiments, we found that the yield of the system is largely based on two main factors: electrode placement and biologic factors.

One major contributing biologic factor to experiment failure was the efficiency in the transient cDNA transfection process used to express the NMDARs. Overall, there was a higher success rate in achieving a high-quality recording from the stably expressing $GABA_AR$ cells (31 successes out of 51 total attempts) than the transiently transfected NMDAR cells (28 successes out of 82 total attempts, Fisher's exact test, $P = 0.0039$). Despite expression of green fluorescent protein, which was coexpressed with NMDAR subunits, 14 of the 42 pulled patches did not have a current response of a sufficient amplitude. By contrast, the $GABA_AR$ cell line had a trend of higher reliability: only five of the 31 outside-out patches failed to have detectable current. This suggests that enhanced yield could result from improved molecular biology methods. Outside of those biologic inefficiencies, monitoring the operation of the $patcherBot_{Pharma}$ suggests that the failures at the gigaseal formation step and the outside-out patch-pulling step are due to slight errors (1–3 μm) in optimally placing the electrode. In this data set, we had performed a subset of experiments in which an experimenter manually intervened by controlling the final placement of the electrode once the $patcherBot_{Pharma}$ had positioned the electrode 100 μm above the next selected cell. In these operator-assisted experiments, we observed that the gigaseal yield was higher, with 97.2%, and the patch-pulling yield was 88.6%. Specifically, in obtaining gigaseals, the operator-assisted trials resulted in 35 successes from 36 attempts compared with nine successes from 15 attempts (Fisher's exact test, $P = 0.0016$). Additionally, in excising outside-out patches, the operator-assisted trials resulted in 31 successes from 35 attempts compared with six successes from nine

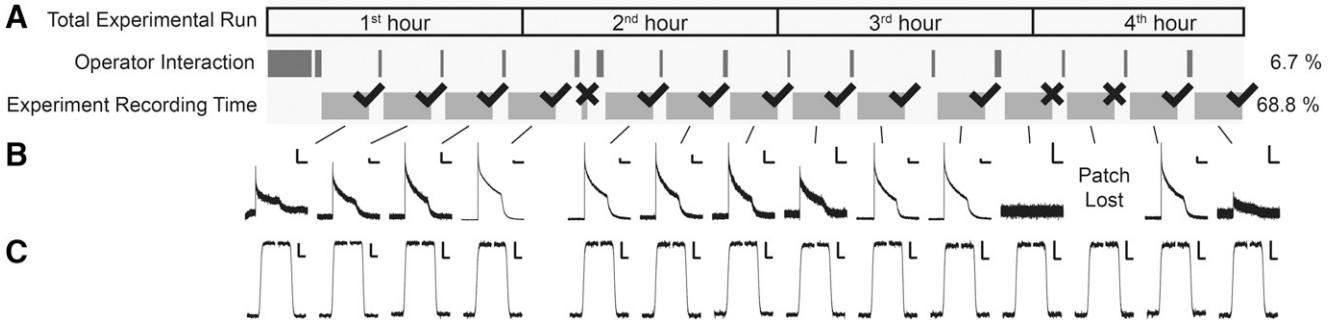

Fig. 4. Representative experimental timeline of patcherBot$_{Pharma}$ operation. (A) Timeline of experimental progress. The time periods of operator interaction with the patcherBot$_{Pharma}$ and recording duration are highlighted, along with recording outcome. (B) GABA$_A$R responses (1 mM GABA, 1-second application) from all successful outside-out patches pulled. Scale bars indicate 20 pA and 0.5 seconds. (C) Post-experiment open-tip position validation utilizing a 50% H_2O/50% wash solution. Scale bars indicate 200 pA and 20 milliseconds. The average [± S.D. (range)] 20–80 rise and fall times for piezoelectric jumps were 3.06 ± 0.78 (1.30 4.11) and 3.56 ± 0.32 (2.27 6.55).

attempts (Fisher's exact test, $P = 0.1383$). The overall yield (successful experiment compared with attempt) of these operator-assisted runs was 69.4% (25 good experiments of 36 attempts), as compared with the ~40% success rate of the other experiments (six good experiments of 15 attempts, Fisher's exact test, $P = 0.0645$). Fully automated electrode placement implemented in the patcherBot$_{Pharma}$ relies on machine vision using camera pixel intensity cross-correlation methods to align a previously stored image of the cell and electrode to make corrections at the beginning of each attempt. These methods work well in placing the electrode somewhere on a cell (~10 μm precision) without operator intervention but lack the accuracy to place it optimally (<1 μm), which appears to have a large impact on overall success. In addition to the losses in efficiency, the machine vision processes are slow because of the necessity to move the electrode or microscope to check for positioning errors. The process time during fully automated patcherBot$_{Pharma}$ operation takes on average 267 ± 35 seconds (mean ± S.D.) to correct the manipulators, land the electrode on the cell, and break in to the whole-cell conformation. This is compared with 74 ± 10 seconds (mean ± S.D.) for the operator-assisted patcherBot$_{Pharma}$, in which robotic translations move the stage to the next cell and place the electrode just above the cell (100 μm) before the operator places the electrode on the cell and, in this case also, forms a gigaseal followed by the automated break-in process. Thus, the patcherBot$_{Pharma}$ can operate fully autonomously, but the speed and performance can be improved by operator intervention during key steps with the current techniques of position error correction.

Operating in this manner, with minor manual interaction, the patcherBot$_{Pharma}$ can collect experiment electrophysiology recordings proficiently, which is demonstrated by a representative run of the patcherBot$_{Pharma}$ from the results mentioned previously (Fig. 4). In this experimental run, the patcherBot$_{Pharma}$ was programmed to collect four-phase recordings. During each phase, five technical replicate sweeps were collected, specifically a 10-second sweep with agonist applied for 0.5 seconds. After each set of recordings, the patch was blown off with high pressure, and the open-tip exchange time was determined to validate the electrode positioning. On average, the recording time and position validation totaled 11.2 minutes. If the patcherBot$_{Pharma}$ detects inadequate patch formation, after the outside-out patch procedure, it terminates the recording and moves on to the next cell, spending only 1.4 minutes in doing so. Over this 3.8-hour recording session, highlighted in Fig. 4, 15 cells were attempted to be patched, yielding 12 successful recording sets. During this time, the operator only interacted with the patcherBot$_{Pharma}$ for 15.5 minutes during recording (7.1% of the experimental run time) after the 10.3 minutes of calibration and cell selection. The patcherBot$_{Pharma}$ was recording data for 2.6 hours, which amounts to 72.0% of the operation time. The GABA$_A$R responses that were collected were of high quality and similar to those previously reported (Fig. 4B; Table 1). Additionally, the placement of the electrode resulted in consistent solution exchange times after each patch recording (Fig. 4C).

Next, we performed a case study (Fig. 5) in which we sought to measure the main actions of a widely used anesthetic, propofol (PRO), to highlight the operational procedure and capability of the patcherBot$_{Pharma}$ in performing an extended, tedious patch-clamp electrophysiology experiment. Propofol's main clinical actions are produced by prolonging

TABLE 1
Summary of activation and deactivation parameters of GABA$_A$R and NMDARs from Figs. 3 and 4. Data shown represent the average ± S.E.M.

		Rapid Application of 1 mM GABA or Glutamate for 1 sec						
		Patch Leak *pA*	Response Peak Amplitude *pA*	Response Steady-State Amplitude *pA*	Desensitization Extent (SS/Peak) %	Desensitization τ *ms*	Deactivation τ *ms*	*N*
GABA$_A$R	+40 mV	24.9 ± 18.7	586 ± 150	170 ± 54	26.4 ± 1.8	681 ± 130	216 ± 29	12
	−60 mV	48.3 ± 36.1	173 ± 48	35.9 ± 13.6	24.8 ± 1.1	965 ± 298	133 ± 6	12
NMDAR GluN2A WT	+40 mV	38.6 ± 32.1	271 ± 104	130 ± 68	34.2 ± 6.4	388 ± 75	71.9 ± 11.0	11
	−60 mV	140 ± 42.6	326 ± 180	215 ± 139	54.8 ± 6.9	984 ± 192	81.3 ± 18.4	7

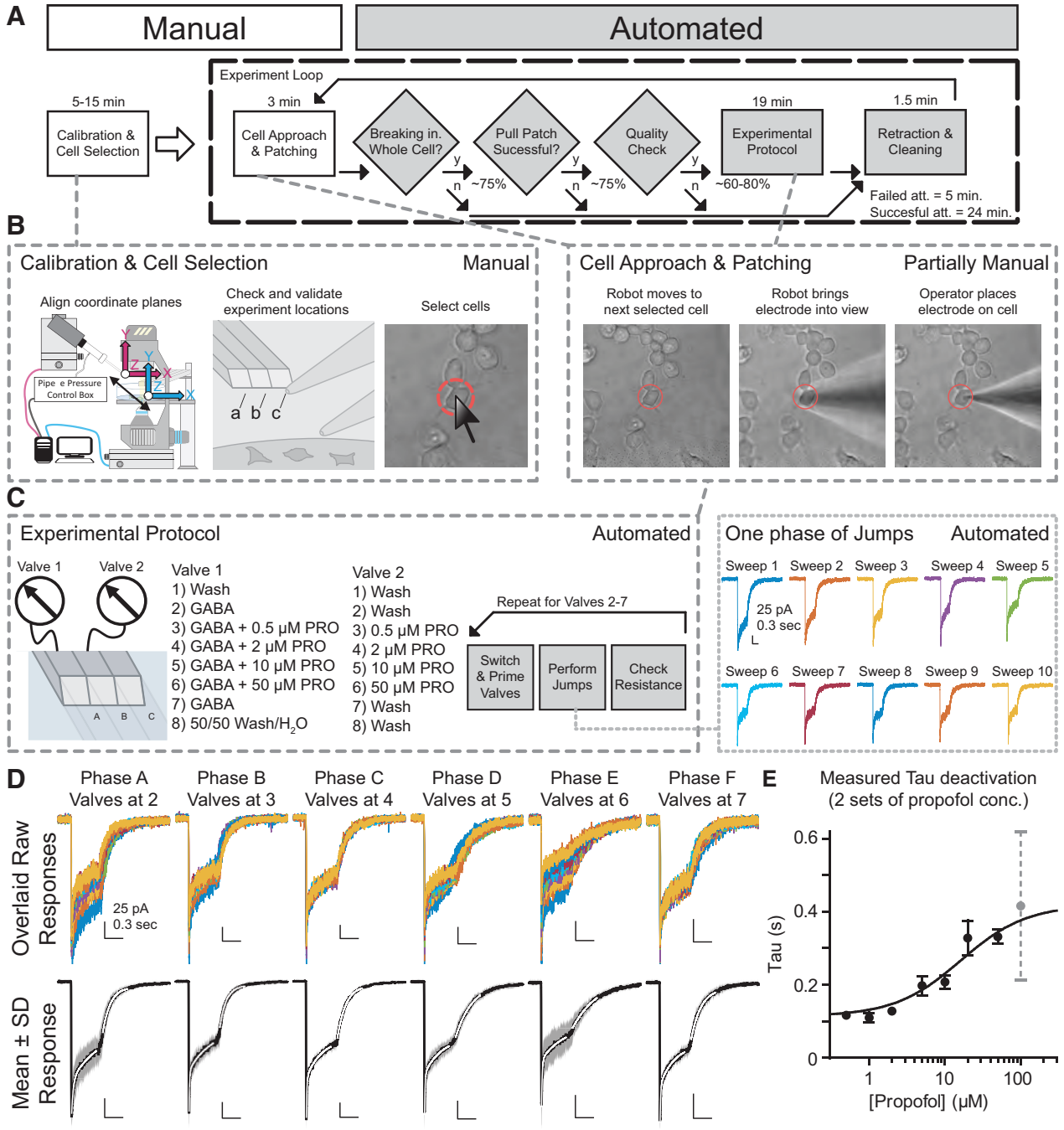

Fig. 5. $GABA_AR$ propofol deactivation time-constant concentration-response case study; the $patcherBot_{Pharma}$ has the capability to collect pharmacological data at an accelerated rate. (A) A flowchart illustrating the $patcherBot_{Pharma}$ operation, timing, and success rate of individual steps. The manual (white boxes) and automated (gray boxes) steps are indicated. After the one-time calibration and cell selection step, the $patcherBot_{Pharma}$ loops through and serially records from the selected cells. Quality control measures are in place to terminate the current experiment and continue to the next iteration. (B) A more detailed depiction of the manual steps is shown. The calibration and cell selection step (left) includes: 1) aligning the electrode and microscope coordinate systems, 2) ensuring the saved locations of the solution manifold are correct, and 3) selecting a set of cells for experimentation (typically 7–12 cells). The cell approach and patching step (right) at the beginning of each loop (coinciding with an auditory signal so that the operator need not always be present) starts when the $patcherBot_{Pharma}$ translates the stage to the next cell selected, and then the electrode is brought to a position just above (100 µm) the cell. The operator then only needs to lower the electrode to the optimal position on the cell and has the option of manually sealing and breaking in or can elect to have the $patcherBot_{Pharma}$ conduct those processes. (C) A more detailed look at the experimental protocol step of the $patcherBot_{Pharma}$ process. In this case, there were six sets of solutions that would be used during each experiment (two control and four propofol solution sets, detailed on the left). Each phase of each experiment would start with the valves changing to the next set to be tested, with a wait step to allow for the solutions to be primed, followed by the collection of 10 replicates of the intended jump protocol (right). (D) The results from one experiment (all phases), showing all replicates (top) and the average (± S.D., shown by shaded gray area) response. The desensitization and deactivation of all recordings were fitted simultaneously and are depicted on the averaged responses (white line). (E) The relationship between the average (± S.E.M.) deactivation τ and propofol concentration is shown and fitted with the Hill equation. The 100 µM propofol response was omitted from fitting because of the reduced response amplitude as a result of the enhanced desensitized state in the presence of such a high concentration of propofol. att., Attempt; conc., concentration.

the deactivation of $GABA_AR$ and have been well characterized (Orser et al., 1994; Adodra and Hales, 1995). We ran the $patcherBot_{Pharma}$ with operator assistance for electrode placement (Fig. 5, A and B) followed by manual patch formation to optimize the time of biologic data collection by the $patcherBot_{Pharma}$. We set out to collect an eight-point concentration-response curve of propofol's effect on $GABA_AR$ deactivation, and we split it into two sets and included a propofol-free control before and after drug application (Fig. 5C). In four half-day recording sessions (two per each concentration set), totaling 12.95 hours of $patcherBot_{Pharma}$ operation, we attempted 42 recordings, obtained 39 gigaseal patches, achieved 28 whole-cell conformations, pulled 24 successful outside-out patches, and completed 18 experiments (including six incomplete) that yielded 113 data points (Fig. 5, D and E; Tables 2 and 3). After eliminating the recordings with too large a leak current, too small a response amplitude, or recording artifacts, we were left with 71 data points that were used to calculate the concentration-response relationship of propofol's ability to prolong the deactivation of $GABA_ARs$ (EC_{50} = 11.8 ± 4.6 μM; Fig. 5, D and E).

Of the 12.95 hours of recording, the operator interacted with the $patcherBot_{Pharma}$ for 2.49 hours, and the $patcherBot_{Pharma}$ collected experimental recordings for 9.07 hours, with an additional 1.39 hours of other automated processing (Table 2). The 2.49 hours of operator interaction includes cell selection, solution maintenance, electrode placement on the cell, and gigaseal formation. In each iteration of the $patcherBot_{Pharma}$ process, it spent 1.99 minutes cleaning the electrode, and the operator spent ~2 to 3 minutes placing the electrode on the cell and establishing the whole-cell conformation. If everything was successful, the $patcherBot_{Pharma}$ would then proceed to collect the experimental data—in total, a 24.6-minute process. If there was an issue with the stability of the patch during the process of pulling the outside-out patch (1.73-minute process), the $patcherBot_{Pharma}$ would clean the electrode and be ready for the next attempt in less than 2 minutes. Although the experiment yield was not overly high (24 of 42 attempts were successful), this did not greatly hinder the performance of the $patcherBot_{Pharma}$ (Table 4). If every patch attempt was successful, the theoretical maximum number of experiments the $patcherBot_{Pharma}$ could have performed in 12.95 hours was 25.8, which is only modestly higher than the 18 that were successfully performed (70% full experiments performed divided by the maximum). Moreover, the rate of data collection, in terms of operator effort, was 2.1 minutes per data point. Should patching efficiency be improved further, the theoretical minimum of operator effort can be reduced to 0.97 minutes per data point.

Discussion

Patch-clamp electrophysiology research is a powerful technique, yet many scientists are dissuaded from learning and utilizing this approach because of its time-consuming nature, in terms of both training and execution. Even for skilled practitioners, the complexity and effort required for comprehensive pharmacology experiments (pharmacological screening or evaluation of full concentration-response relationships) can be impractical. Here, we have demonstrated the capabilities of the $patcherBot_{Pharma}$ for ligand-gated ionotropic receptor pharmacological screening, which makes patch-clamp electrophysiology experimentation rapid, less skill intensive, and more reliable. The automation of the $patcherBot_{Pharma}$—namely, precise and accurate electrode translations, solution handling, electrode cleaning, and rapid solution exchange—greatly expands the repertoire of experiments that the patcherBot can perform. This allows one to conduct nearly any pharmacological experiment typically performed on ligand-gated or voltage-gated ion channels using the $patcherBot_{Pharma}$ (e.g., Supplemental Figs. 1 and 2). Additionally, the $patcherBot_{Pharma}$ has the flexibility to be retooled as needed based off a traditional patch-clamp rig and can run autonomously or with minimal operator intervention to suit the experimental situation. Thus, the $patcherBot_{Pharma}$ could be set up to patch adherent cells and applied compounds via the bath input, if desired, and the full automated capabilities of the system will be retained if all test compounds can be fully washed out.

The $patcherBot_{Pharma}$ has a very high yield (80%–100%) of obtaining giga-ohm resistance patches and of breaking in to achieve the whole-cell patch conformation. The methods we have employed to lift isolated patch-clamped cells and to pull outside-out patches are highly reliable (70%–90% yield). These capabilities allow the $patcherBot_{Pharma}$ to spend more time performing the intended electrophysiology experiment and less time in the process of manually guiding the position of the patch electrode throughout the course of the full experiment. With this improved system, the primary determinants for whether a particular experimental attempt concludes in a

TABLE 2
Census of robotic operation and operator interaction time for the propofol case study

	Total Operation	Electrode Cleaning (Robotic Control)	Data Collection (Robotic Control)	Patch Establishment (Operator Control)	Nonrecording Time[a]
Total time	12.95 h	1.39 h	9.07 h	2.49 h	3.88 h
(percent)		(10.7%)	(70.0%)	(19.3%)	(30%)
Time per cycle (successful cycle)		1.99 min	24.6 min	3.55 min	5.54 min
Time per data point (successful cycle)			4.1 min[b]	2.1 min[c]	

[a]The nonrecording time is the time the robot is not performing the data collection protocol.
[b]Each data collection phase equals the solution change time (~1 min solution change time) plus the data collection time (1.67 min data collection); however, the mean time per data point reflects the additional time needed to pull the patch and validate the jump at the end of the experiment averaged into the timing for each phase.
[c]This rate represents the total time the operator spent interacting with the $patcherBot_{Pharma}$ during the entire experiment performance (cell selection, solution maintenance, electrode placement on the cell, and gigaseal formation). The theoretical maximal efficiency of data collection per the operator's effort would be 0.97 min of the operator's time per data point.

TABLE 3
Concentration-response of propofol on $GABA_AR$ activation and deactivation. Data shown represent the average ± S.E.M.

$GABA_AR$	Patch Leak *pA*	Response Peak Amplitude *pA*	Response Steady-State Amplitude *pA*	Desensitization Extent (SS/Peak) *%*	Deactivation τ *ms*	*N*
Rapid application of 1 mM GABA for 0.5 sec: propofol concentration set 1						
GABA control	20.9 ± 7.3	133 ± 36	51.1 ± 12.3	39.3 ± 2.0	129 ± 11	8
0.5 μM PRO	28.9 ± 13.5	100 ± 20	40.4 ± 8.9	39.6 ± 1.3	116 ± 13	8
2 μM PRO	16.7 ± 4.5	109 ± 32	45.6 ± 14.9	40.0 ± 1.7	128 ± 13	6
10 μM PRO	18.8 ± 4.8	96.0 ± 25.2	42.1 ± 11.6	43.1 ± 2.2	208 ± 20	6
50 μM PRO	16.0 ± 3.0	63.9 ± 17.8	23.5 ± 7.4	33.8 ± 2.7	331 ± 21	7
PRO washout	15.9 ± 2.8	66.7 ± 22.6	29.2 ± 11.3	41.8 ± 1.7	143 ± 25	6
Rapid application of 1 mM GABA for 0.5 sec: propofol concentration set 2						
GABA control	30.6 ± 6.2	93.6 ± 6.8	30.5 ± 8.1	31.8 ± 7.7	130 ± 27	6
1 μM PRO	36.5 ± 6.4	72.2 ± 18.0	24.2 ± 6.6	34.9 ± 6.7	110 ± 15	6
5 μM PRO	34.3 ± 8.2	37.8 ± 9.1	11.1 ± 2.4	30.0 ± 5.1	198 ± 29	5
20 μM PRO	42.1 ± 8.0	21.5 ± 4.6	6.1 ± 2.2	25.2 ± 6.6	328 ± 53	5
100 μM PRO	29.0 ± 5.9	8.9 ± 1.2	5.8 ± 7.5	—	415 ± 226	5
PRO washout	24.8 ± 10.1	20.1 ± 6.3	5.3 ± 3.4	25.2 ± 13.5	129 ± 12	3

successful recording relies more on biologic factors than robotic or operator factors. In our experiments with heterologous expression systems (namely, transfected HEK cells), the yield in high-quality recordings, with high receptor expression, of the $patcherBot_{Pharma}$ reaches 60%–70% of the cells attempted. With this high efficiency of data collection, we could rapidly replicate previous data sets by reducing the time it takes to produce an eight-point concentration-response curve of the effects of propofol on $GABA_AR$ deactivation from weeks or months of recording down to ~13 hours of recording.

This system retains the full capabilities of traditional electrophysiology rigs. We observed solution exchange times, with our larger three-barreled manifold, in the low millisecond range (~1 to 2 milliseconds), which could be reduced further (<1 millisecond) using different solution manifolds (Glasgow and Johnson 2014; MacLean 2016). This allows for accurate experimentation and can be used to study rapidly desensitizing receptors, which cannot be measured on commercially available multiwell high-throughput patch-clamp instrumentation. The $patcherBot_{Pharma}$ system largely comprises typical components of a conventional electrophysiology rig (Supplemental Table 2) and thus does not require a substantial or prohibitive cost to upgrade. Running costs are low, comparable to the cost of operating a traditional patch-clamp rig, and primarily include the cost of the preparation (cell culture costs) and compounds being evaluated. There are no additional changes in running costs based on each data point collected, except for reduced glass consumption and perhaps reduced preparation costs that come with more efficient recording. However, as the $patcherBot_{Pharma}$ can be in operation for extended periods of time and can execute experiments at a high rate, the running costs based on each day of operation may, in fact, be higher as a result of the increased bath solution usage and increased use of pharmacological compounds.

TABLE 4
Performance of the $patcherBot_{Pharma}$ in the propofol case study

	Counts	Yield	Theoretical Max.[a]
	N	*%*	*N*
Patch attempts	42		
Successfully established gigaseals	39	93	
Whole-cell conformations obtained	28	72	
Outside-out patches obtained	24	86	
Experiments started	24	—	
Successful experiments	18	75	25.8
Total data points collected	113		154.8
Data points passed quality control	71		

[a]The theoretical maximum (max.) values were determined by taking the total operation time divided by the total time for one successful cycle. Since there are six collected data points per experiment, the theoretical maximum for total collected data points equals the number of experiments multiplied by a factor of 6.

There are several improvements to the $patcherBot_{Pharma}$ that could further increase its capabilities and productivity. Enhanced machine vision correction methods could allow for more precise placement of the electrode with less computation time thus increasing the unattended success rate and reducing human effort. Algorithms for cell detection could be employed to make cell selection agnostic, with further reduction in human effort and bias (Yip et al., 2021). Systematic collection of data will aid in meta-analysis of experiments, which could identify unrecognized factors that influence experimental results or experimental variability.

The $patcherBot_{Pharma}$ facilitates pharmacological experimentation on ligand-gated channels through increased productivity and the ability to address labor-intensive questions (collecting multiple concentration data points or testing more constructs). This allows more complex experimental protocols that include increased number of replicates and more controls. Many neuroscience studies have been cited as having low power in their experimental design (Button et al., 2013), which could be rectified by utilizing the $patcherBot_{Pharma}$. Additionally, the $patcherBot_{Pharma}$ reduces the chance of human bias when collecting data, as the experiment protocols are explicitly defined prior to experiment execution. Moreover, methods to introduce blinding in the experimental design could be employed along with automated analysis to allow one to easily jump to the final analyzed data point after conducting the experiment. The data collected by the $patcherBot_{Pharma}$ might be more reproducible due to enhanced transparency, as the full $patcherBot_{Pharma}$ experiment data log could be documented along with the results (Munafò et al.,

2017). With the reduction in human effort that comes with operating the patcherBot$_{Pharma}$, it becomes feasible that a single person could operate multiple patcherBot$_{Pharma}$ at once for increased data collection. In summary, the patcherBot$_{Pharma}$ enhances the capabilities of a researcher utilizing patch-clamp approaches by decreasing operator interaction time, reducing human bias, increasing experiment yield, allowing more complicated experimental design, and enabling experiments that require high volumes of recordings.

Acknowledgments

We would like to thank Jing Zhang and Anling Kaplan for excellent technical assistance.

Authorship Contributions

Participated in research design: Perszyk, Yip, Jenkins, Traynelis, Forest.

Conducted experiments: Perszyk, Yip, McConnell.

Contributed new reagents or analytic tools: Perszyk, Yip, McConnell, Wang.

Performed data analysis: Perszyk, McConnell, Yip.

Wrote or contributed to the writing of the manuscript: Perszyk, Yip, McConnell, Wang, Jenkins, Traynelis, Forest.

References

Adodra S and Hales TG (1995) Potentiation, activation and blockade of GABAA receptors of clonal murine hypothalamic GT1-7 neurones by propofol. *Br J Pharmacol* **115**:953–960.

Ai HW (2015) Fluorescent-protein-based probes: general principles and practices. *Anal Bioanal Chem* **407**:9–15.

Annecchino LA, Morris AR, Copeland CS, Agabi OE, Chadderton P, and Schultz SR (2017) Robotic automation of in vivo two-photon targeted whole-cell patch-clamp electrophysiology. *Neuron* **95**:1048–1055.e3.

Auerbach A and Zhou Y (2005) Gating reaction mechanisms for NMDA receptor channels. *J Neurosci* **25**:7914–7923.

Button KS, Ioannidis JPA, Mokrysz C, Nosek BA, Flint J, Robinson ESJ, and Munafò MR (2013) Power failure: why small sample size undermines the reliability of neuroscience. *Nat Rev Neurosci* **14**:365–376.

Campagnola L, Kratz MB, and Manis PB (2014) ACQ4: an open-source software platform for data acquisition and analysis in neurophysiology research. *Front Neuroinform* **8**:3.

Chakrapani S, Cordero-Morales JF, Jogini V, Pan AC, Cortes DM, Roux B, and Perozo E (2011) On the structural basis of modal gating behavior in K(+) channels. *Nat Struct Mol Biol* **18**:67–74.

Colquhoun D and Sigworth FJ (1995) Fitting and statistical analysis of single-channel records, in *Single-Channel Recording* (Sakmann B and Neher E, eds) pp 483–587, Springer US, Boston, MA.

Deo C and Lavis LD (2018) Synthetic and genetically encoded fluorescent neural activity indicators. *Curr Opin Neurobiol* **50**:101–108.

Glasgow NG and Johnson JW (2014) Whole-cell patch-clamp analysis of recombinant nmda receptor pharmacology using brief glutamate applications, in *Patch-Clamp Methods and Protocols* (Martina M and Taverna S, eds) pp 23–41, Springer New York, New York, NY.

Kodandaramaiah SB, Franzesi GT, Chow BY, Boyden ES, and Forest CR (2012) Automated whole-cell patch-clamp electrophysiology of neurons in vivo. *Nat Methods* **9**:585–587.

Kolb I, Landry CR, Yip MC, Lewallen CF, Stoy WA, Lee J, Felouzis A, Yang B, Boyden ES, Rozell CJ, et al. (2019) PatcherBot: a single-cell electrophysiology robot for adherent cells and brain slices. *J Neural Eng* **16**:046003.

Kolb I, Stoy WA, Rousseau EB, Moody OA, Jenkins A, and Forest CR (2016) Cleaning patch-clamp pipettes for immediate reuse. *Sci Rep* **6**:35001.

Liu C, Li T, and Chen J (2019) Role of high-throughput electrophysiology in drug discovery. *Curr Protocols Pharmacol* **87**:e69.

MacLean DM (2016) Constructing a rapid solution exchange system, in *Ionotropic Glutamate Receptor Technologies* (Popescu GK, ed) pp 165–183, Springer New York, New York, NY.

Mollinedo-Gajate I, Song C, and Knöpfel T (2019) Genetically encoded fluorescent calcium and voltage indicators. *Handb Exp Pharmacol* **260**:209–229.

Munafò MR, Nosek BA, Bishop DVM, Button KS, Chambers CD, Percie du Sert N, Simonsohn U, Wagenmakers E-J, Ware JJ, and Ioannidis JPA (2017). A manifesto for reproducible science. *Nat Hum Behav* **1**: 0021.

Neher E and Sakmann B (1976) Single-channel currents recorded from membrane of denervated frog muscle fibres. *Nature* **260**:799–802.

Obergrussberger A, Goetze TA, Brinkwirth N, Becker N, Friis S, Rapedius M, Haarmann C, Rinke-Weiß I, Stölzle-Feix S, Brüggemann A, et al. (2018) An update on the advancing high-throughput screening techniques for patch clamp-based ion channel screens: implications for drug discovery. *Expert Opin Drug Discov* **13**:269–277.

Orser, B., L. Wang, P. Pennefather and J. MacDonald (1994). Propofol modulates activation and desensitization of GABAA receptors in cultured murine hippocampal neurons. **14**: 7747–7760.

Perszyk RE, Swanger SA, Shelley C, Khatri A, Fernandez-Cuervo G, Epplin MP, Zhang J, Le P, Bülow P, Garnier-Amblard E, et al. (2020) Biased modulators of NMDA receptors control channel opening and ion selectivity. *Nat Chem Biol* **16**:188–196.

Suk H-J, Boyden ES, and van Welie I (2019) Advances in the automation of whole-cell patch clamp technology. *J Neurosci Methods* **326**:108357.

Suter BA, O'Connor T, Iyer V, Petreanu LT, Hooks BM, Kiritani T, Svoboda K, and Shepherd GM (2010) Ephus: multipurpose data acquisition software for neuroscience experiments. *Front Neural Circuits* **4**:100.

Wu Q and Chubykin AA (2017) Application of automated image-guided patch clamp for the study of neurons in brain slices. *J Vis Exp* **125**:56010.

Yip MC, Gonzalez MM, Valenta CR, Rowan MJM, and Forest CR (2021) Deep learning-based real-time detection of neurons in brain slices for in vitro physiology. *Sci Rep* **11**:6065.

Yu HB, Li M, Wang WP, and Wang XL (2016) High throughput screening technologies for ion channels. *Acta Pharmacol Sin* **37**:34–43.

Address correspondence to: Craig R. Forest, 315 Ferst Dr. NW Rm. 1310, Atlanta, GA 30332. E-mail: cforest@gatech.edu; Andrew Jenkins, Department of Pharmacology and Chemical Biology, 1510 Clifton Rd., Atlanta, GA 30322. E-mail: ajenki2@emory.edu; or Stephen F. Traynelis, Department of Pharmacology and Chemical Biology, 1510 Clifton Rd. NE, Atlanta, GA, 30322. E-mail: strayne@emory.edu.